CHAPTER 23

INTERACTION OF WAVES AND A TURBULENT CURRENT

by

J. D. A. van Hoften[1] and S. Karaki[2]

ABSTRACT

An experimental investigation was made to study wave-current interaction. Wave amplitude attenuation was measured along a laboratory wave channel to compare wave dissipation with and without flow. Mean, wave, and turbulent velocities were also measured to determine the modifications of the flow imposed by the gravity waves propogating with the current. The process of energy transfer in the wave-current system was studied. Energy was found to be extracted from the waves, diffused downward and dissipated by an increase in bottom shear stress.

INTRODUCTION

The development of a model to accurately describe the generation and decay of ocean surface waves has been a primary objective of oceanographers for decades. In present wave forecasting formulas there is far more agreement on empirical wave growth than on wave dissipation. Numerous studies have dealt with the aspect of laminar wave energy dissipation such as the early theoretical work of Lamb (1932) and Hunt (1952). Experimentally, a large variety of studies have been made relating wave dissipation to near-surface viscous effects or to the oscillatory boundary layers. In real situations, waves seldom travel across non-turbulent waters. Thus an account must be made of the interaction which results as orbital wave velocities work against the shear current and turbulence which likely exist.

This paper describes a laboratory study of the interaction of waves and current as mechanically generated, monochromatic, intermediate-depth gravity waves propogate on a turbulent open channel flow. The two areas of primary concern are:

1. Wave modification - the change in wave form, mainly wave amplitude, resulting in increased wave energy dissipation.

2. Current modification - the alteration of mean and turbulent flow parameters due to the wave interactions, as well as changes in the resistance to flow and energy transport properties.

[1]Assistant Professor of Civil Engineering, University of Houston, Houston, Texas (Formerly Research Assistant, Colorado State University)

[2]Professor of Civil Engineering, Colorado State University, Fort Collins, Colorado

THEORETICAL ANALYSIS

In order to create a set of baseline data for wave attenuation analysis, it is first necessary to examine wave energy dissipation without the effect of channel flow. Hunt (1952) utilized the basic laminar wave dissipation equations and integrated the effects of the oscillatory boundary losses for the side and bottom and derived an expression for a wave attenuation modulus,

$$\alpha = \frac{2k}{b}\sqrt{\frac{\nu}{2\sigma}}\left(\frac{kb + \sinh 2kh}{2kh + \sinh 2kh}\right) \tag{1}$$

where b is channel width, h is flow depth, k is wave number (2π/wave length), ν is kinematic viscosity and σ is wave frequency (2π/period) derived from $\sigma^2 = gk \tanh kh$. Wave amplitude attenuation is then defined by the exponential form

$$a = a_o e^{-\alpha x} \tag{2}$$

where a_o is the initial wave amplitude and a is the attenuated amplitude at distance x.

The analysis of the wave-current amplitude attenuation utilizes a control volume of unit width bounded by upstream and downstream vertical sections, the channel bottom and the free water surface. Whitham (1962) applied the concept of the radiation stress (introduced by Longuet-Higgins and Stewart (1960)) to the momentum and energy flux in water waves. Application of Whitham's concepts to the case of attenuating monochromatic waves propogating on a uniform open channel flow begins with the integral momentum equation,

$$\frac{d}{dx}(\rho h U_m^2) + \rho g h \sin\theta + \frac{dS_{xx}}{dx} = -\bar{\tau}_b \tag{3}$$

where $S_{xx} = E\left(\frac{2kh}{\sinh 2kh} + \frac{1}{2}\right)$ (4)

is the longitudinal component of radiation stress, $\sin\theta$ is channel slope, $\bar{\tau}_b$ is the mean bottom shear stress, a is wave amplitude, E is wave energy density ($1/2\ \rho g a^2$), and U_m is the mass transport velocity defined by

$$U_m = \bar{u} + \frac{E}{\rho h c} \tag{5}$$

where $\bar{u}$ is mean uniform flow velocity, and c is phase speed. By substituting equations (4) and (5) into (3), differentiating and retaining terms to the order of a^2 and assuming an exponential wave attenuation of the form of equation (2), the resulting equation for bottom shear stress is

$$\bar{\tau}_b = \rho g h \sin\theta + \rho g \alpha a^2 \left[\frac{2}{c}(\bar{u} + c_g) - \frac{1}{2}\right] \quad (6)$$

where c_g is the group velocity defined by

$$c_g = \frac{C}{2}\left[1 + \frac{2kh}{\sinh 2kh}\right] \quad (7)$$

Note that for $\theta = 0$, and $\bar{u} = 0$, equation (6) reduces to the form

$$\bar{\tau}_b = \rho g \alpha a^2 \left[\frac{2c_g}{C} - \frac{1}{2}\right] \quad (8)$$

which is just dS_{xx}/dx. In other words for the case of waves on still water the shear stress on the bottom is balanced by the rate of change of the radiation stress. Also note that if $\theta \neq 0$, $\bar{u} \neq 0$, and $\alpha = 0$, or the case of waves propagating on a current without attenuation,

$$\bar{\tau}_b = \rho g h \sin\theta \quad (9)$$

which is the bottom shear stress without waves.

In the same manner, the equation for the energy flux through the control volume is

$$\frac{d}{dx}\left[\frac{\rho h U_m^3}{2} + \rho g h^2 U_m + S_{xx} U_m + E U_m + E c_g\right] = -D \quad (10)$$

where D is the energy dissipation defined as dE/dt. Again substituting and retaining terms of the order a^2 gives the total dissipation as

$$D = \rho g h \sin\theta\, \bar{u} + E\left[\frac{g \sin\theta}{c} + \alpha\bar{u}\left(1 + \frac{3\bar{u}}{c}\right) + 2\alpha c_g\left(1 + \frac{2\bar{u}}{c}\right)\right] \quad (11)$$

The first term on the right is the energy dissipation due to channel flow alone as the product of shear stress and mean velocity. The remaining terms represent the additional dissipation due to wave-current interaction and will be denoted D_w. For the case of no flow, $\bar{u} = 0$, $\theta = 0$, and noting that $da/dx = -\alpha a$, equation (11) reduces to

$$D = c_g \rho g \alpha a^2 \quad (12)$$

or

$$D = -c_g \frac{dE}{dx} \quad (13)$$

Thus the energy dissipation in still water is a product of the group velocity and the longitudinal wave energy density gradient.

The above analysis provides a basis for the experimental measurements. Terms of equation (11) may be directly measured and an estimate may be computed for the total dissipation between successive sections of the channel. Limitations are imposed by the

assumption of a uniform velocity profile and the neglect of side-wall losses. Also neglected is the integral effect of the turbulent interaction. A possible improvement may be made to the analysis by the use of the energy equation derived by Brink-Kjaer and Jonsson (1975) which assumes a linear shear profile.

EXPERIMENTAL APPARATUS AND PROCEDURES

Figure 1 shows a schematic of the wind-wave facility at Colorado State University. The flume is 15.8 m long, 60 cm wide and 70 cm deep. Flow was recirculated at a constant depth of 15.2 cm and waves were generated by a vertical plunger of the upstream end. Mean flow velocities ranged from 15.0 to 60.0 cm/sec and wave frequencies varied from 1.3 to 2.5 Hz.

An initial study of wave attenuation in still water was made to compare the experimental results to the theoretical laminar dissipation of equation (1). Water surface elevations were measured with a capacitance probe mounted on a moving carriage. Average or rms wave heights were measured at 15 cm intervals along the centerline of the 10 m test section. Wave lengths were measured directly by longitudinally separating two capacitance probes and observing the corresponding Lissajous figure on an X-Y oscilloscope plot. Integral wave locations were recorded when the figure repeated itself.

Waves were next generated on a series of steady currents and wave profiles were measured. Artificial bottom roughness elements assured a fully developed turbulent flow. Velocity measurements were made with a split hot-film anemometer at various depths in the flow field both with and without waves. Simultaneous wave and velocity data were digitized and stored on magnetic tape.

Iterative computer techniques were used to analyze the split-film data due to the large intensities of the velocity fluctuations. Phase averaging techniques were next used to compute flow quantities relative to the average wave profile. Quantities computed at each depth included mean velocity, wave velocity, longitudinal and vertical turbulence intensities, and turbulent and wave induced Reynolds stress.

To separate the velocity components the instantaneous velocity, u_i, is written as a sum of a time mean, $\bar{u}_i$, a wave induced component, $\tilde{u}_i$, and a random component, u_i . Thus

$$u_i(x,z,t) = \bar{u}_i(x,z) + \tilde{u}_i(x,z,t) + u_i \quad (x,z,t) \quad i = 1,2 \quad (14)$$

By first time averaging, the mean signal is removed. The process of phase averaging then identities wave induced and turbulent velocities as a function of wave phase. Phase averaging is symbolized by brackets ($\langle \cdot \rangle$).

WAVE MODIFICATION

Figure 2 shows three typical mean wave amplitude variation curves for waves in still water. Figure 3 illustrates similar measurements for waves on a flowing channel. The rms amplitudes are normalized by the amplitude at the beginning of the test section. Reflected wave energy creates the regular variation in rms wave amplitude throughout the channel. In most still water cases the pattern obeyed the one-half wave length theory presented by Ursell et.al. (1959). For waves on a current the pattern was distorted due to the modification of wave parameters by the flow, but a regular sinusoidal pattern still existed in the channel.

Attenuation, or wave energy dissipation is demonstrated by the gradual decay of wave amplitude along the channel. The measured exponential decay modulus, α_m, was calculated by a least squares fit of equation (2) to the measured profiles. It is readily apparent that neglecting wave reflection would seriously affect attenuation measurements. Figure 4 is a plot of representative measured attenuation coefficients on still water against the viscous theory of Hunt (1952). In nearly all cases the theory slightly underestimates the measured attenuation modulus, a fact that many investigators have previously noted (Eagleson (1962), and Grosch et.al. (1960)).

In order to compare wave attenuation on still and moving water it is necessary to analyze the wave-current results from a reference system convected with the mean velocity. The results then show a reduced relative frequency and decreased fetch. Figure 5 shows wave dissipation as a function of wave amplitude on still water. Note again that the dissipation is slightly underestimated by viscous theory but increases nearly as the square of the amplitude. Figure 6 is a similar plot of waves on a current, where D_w is the wage dissipation from the convected reference system, calculated from equation (11). Note in this case the large increase in wave dissipation due to the wave-current interaction and the divergence from the a^2 variation as amplitude increases. Figure 7 shows the dissipation as a function of wave steepness, ak, with mean velocity, $\bar{u}$, as a third variable, Steeper waves on the same flow are shown to dissipate energy faster, probably due to the added-stretching of vortex lines as described by Phillips (1959).

FLOW MODIFICATION

Figure 8 illustrates the effect on the velocity profile of increasing frequency and amplitude of waves superposed on a constant mean velocity. Mean velocities at each relative depth, z/h, are normalized by the bulk mean velocity. As the frequency and amplitude increase, the mean velocity profile flattens near the surface and steepens near the bottom. Equation (16) predicts that $\bar{\tau}_b$ will increase as the wave amplitude and attenuation modulus increase. The increase in velocity gradient near the bottom indicates the relative increase in average boundary shear.

The modification of mean velocity and turbulence quantities for a typical run is shown in Figure 9. Dotted profiles are those measured without waves. Quantities for the wave-current profiles are an average over a wavelength of the phase averaged results. The mean velocity profiles indicate a strong interaction with a large increase in gradient near the bottom. The local longitudinal and vertical turbulence intensities show an increase near the surface and relative reduction in the middle regions. The Reynolds stress becomes positive near the surface due to the reversal of the mean velocity gradient, and its magnitude is lower throughout the depth. It is apparent that the interaction of the waves and shear flow produce turbulence near the surface and that it diffuses downward, likely through the action of wave induced pressure terms. A further analysis of the energy transfer mechanism is given in van Hoften (1976).

Local flow characteristics give insight into the magnitude of the interaction. Figure 10 shows the longitudinal wave induced velocity at various relative depths. Velocity variations are typical of intermediate-depth waves with finite velocities near the bottom. Figure 11 is a plot of the phase averaged longitudinal turbulence intensity and Figure 12 is the turbulent Reynolds stress. Note that both exhibit double frequency behavior and both become less phase dependent as depth increases.

One-dimensional energy spectra of the longitudinal velocity fluctuation, with and without waves, were computed. Figure 13 shows spectra computed at four relative depths without waves. The inertial subrange where the slope obeys the -5/3 law appears as a narrow band due to the relatively low flow Reynolds number (R_e = 36,900). The high frequency portions of the spectra conform closely to the -7 slope where viscous effects determine energy transfer. A -1 slope at z/h = 0.07 is mildly indicated in the region where Tchen (1953) predicts large turbulence production, near solid boundaries. Figure 14 shows spectra of the total longitudinal velocity (u + u') with waves. The large peaks in the plots correspond to the wave induced velocity component at 1.88 Hz. Note that relative peaks decrease with depth, as the velocity plots from Figure 10 indicate. The spectrum at z/h = 0.95 appears to have a range of low frequencies where the -1 slope applies, representing a production range. Chang and Cheng (1972) studied turbulent airflow over water waves and predicted that the -1 power law should apply from the dominant wave frequency to the lower bound of the inertial subrange. The low Reynolds number of the present flows, however, prevents an accurate assessment of this concept.

CONCLUSIONS

Waves propagating on an open channel flow are shown to be altered by a combination of the interaction of the waves with the shear gradient and the existing turbulence. The effect is to extract energy from the waves resulting in an increased wave attenuation.

The flow itself is altered by the superposed waves. The induced orbital wave velocities distort the mean velocity profile increasing the gradient near the bed. Turbulence energy is produced near the surface by the interaction of the wave induced Reynolds stresses and the fluctuating velocity gredients. The energy diffuses downward where it is dissipated on the bottom by an increase in apparent boundary shear stress.

REFERENCES

Brink-Kjaer, O. and I.G. Jonsson (1975), Radiation Stress and Energy Flux in Water Waves on a Shear Current. Progress Report 36, Inst. Hydrodyn. and Hydraulic Engineering, Tech. University of Denmark, p 27.

Chang, P.C., and I.M. Cheng (1972), Interaction Subrange Spectrum of Turbulent Wind Over the Air Water Interface. J. Physical Oceanography, 2, p 273.

Eagleson, P.S. (1962), Laminar Damping of Oscillatory Waves. J. Hydraulics Div., ASCE, HY3, May, p 155.

Grosch, C.E., L.W. Wood, and S.J. Lukesik (1960), Viscous Dissipation of Shallow Water Waves. Physics of Fluids, 3, No. 3, p 477.

Hunt, J.N. (1952), Viscous Damping of Waves Over an Inclined Bed in a Channel of Finite Width. LaHouille Blanche, December, p 836.

Lamb, H. (1932), Hydrodynamics, Dover Pub. Inc., New York.

Longuet-Higgins, M.S., and R.W. Stewart (1960), Changes in the Form of Short Gravity Waves on Long Waves and Tidal Currents. J. Fluid Mechanics, 8, p 565.

Tchen, C.M. (1953), The Spectrum of Energy in Turbulent Shear Flows. J. Research, National Bureau of Standards, Vol. 50, p 51.

Ursell, F., R.G. Dean, and Y.S. Yu (1960), Forced Small Amplitude Water Waves: A Comparison of Theory and Experiment. J. Fluid Mechanics, 7, p 33.

van Hoften, J.D.A. (1976), The Interaction of Gravity Waves and Turbulent Channel Flow, Ph.D. Dissertation, No. CED75-76JDAvH36, Colorado State U., Ft. Collins.

Whitham, G.B. (1962), Mass, Momentum and Energy Flux in Water Waves. J. Fluid Mechanics, 12, p 135.

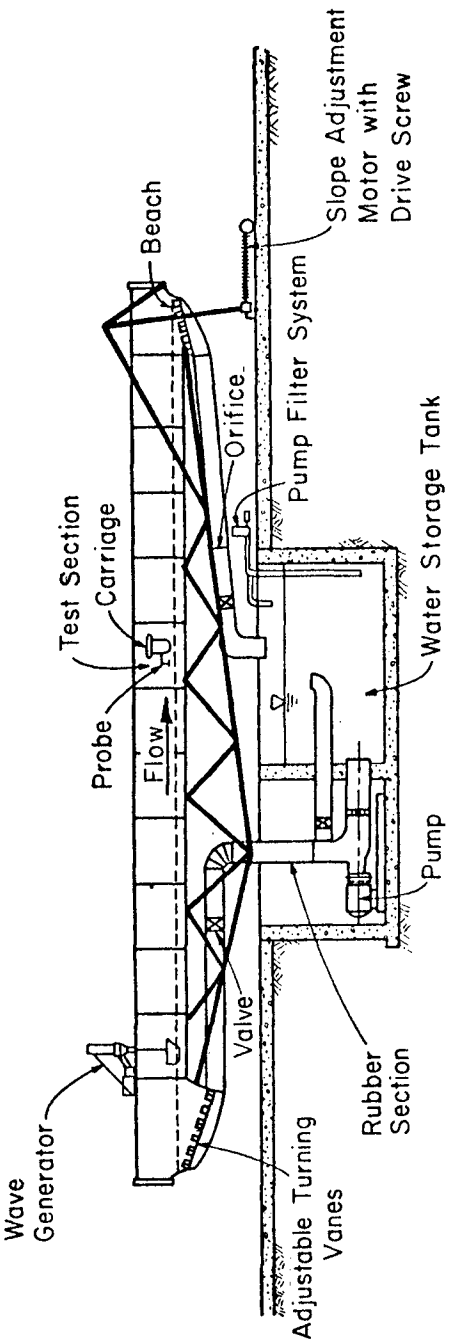

Figure 1. Wind-wave facility of Colorado State University.

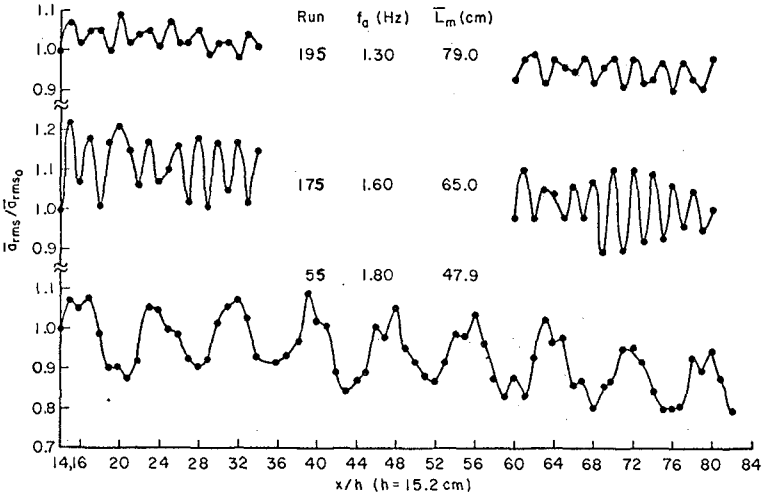

Figure 2. Still water reflection and attenuation profiles

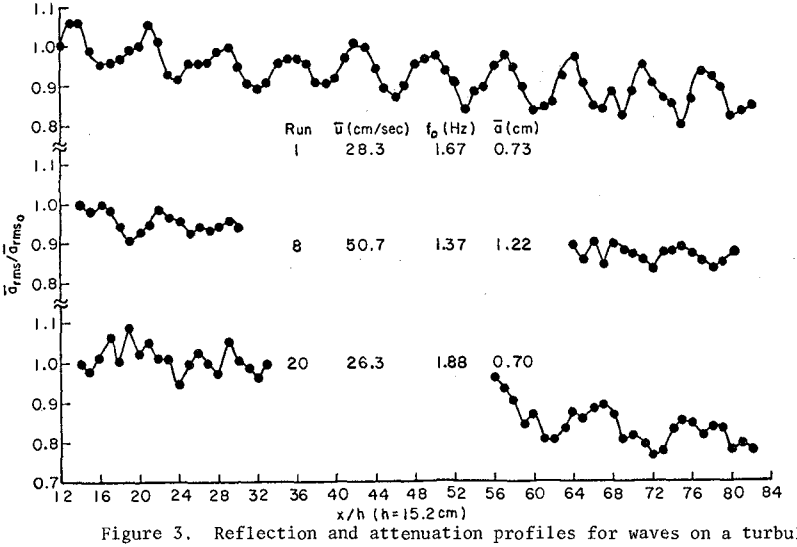

Figure 3. Reflection and attenuation profiles for waves on a turbulent current.

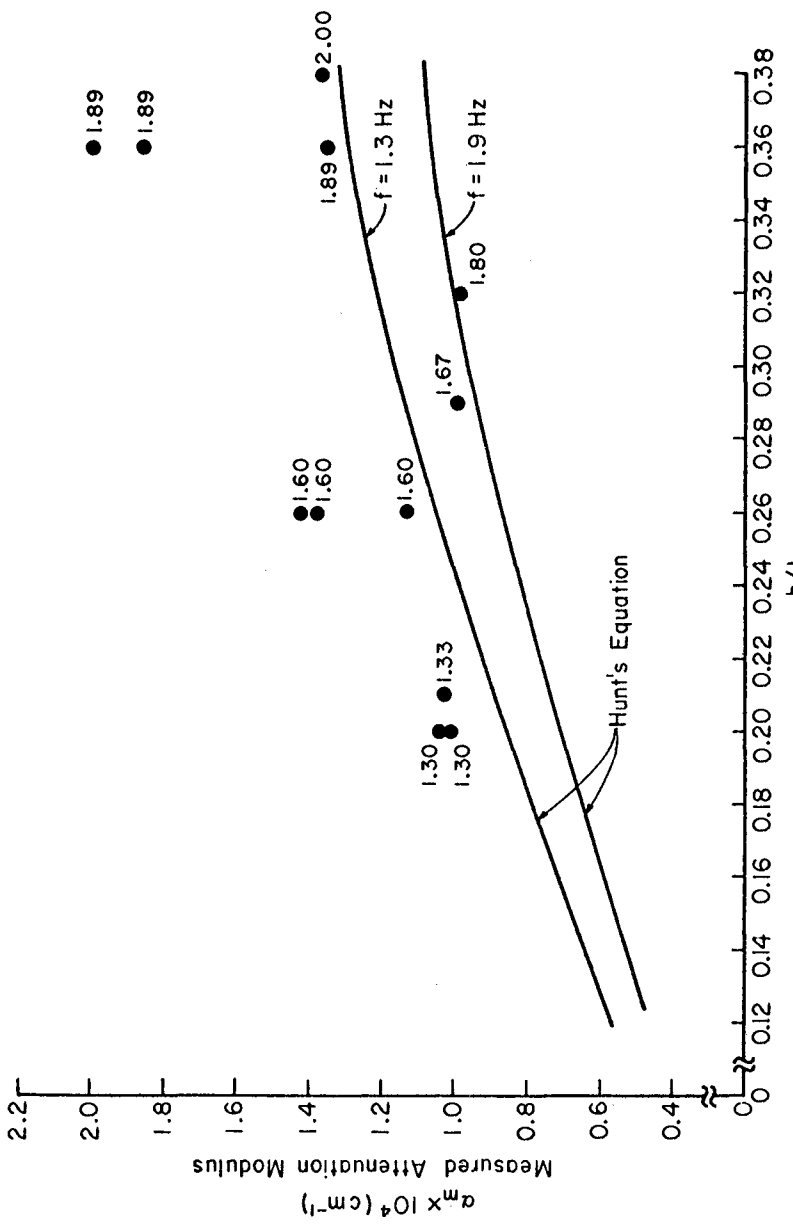

Figure 4. Measured attenuation modulus.

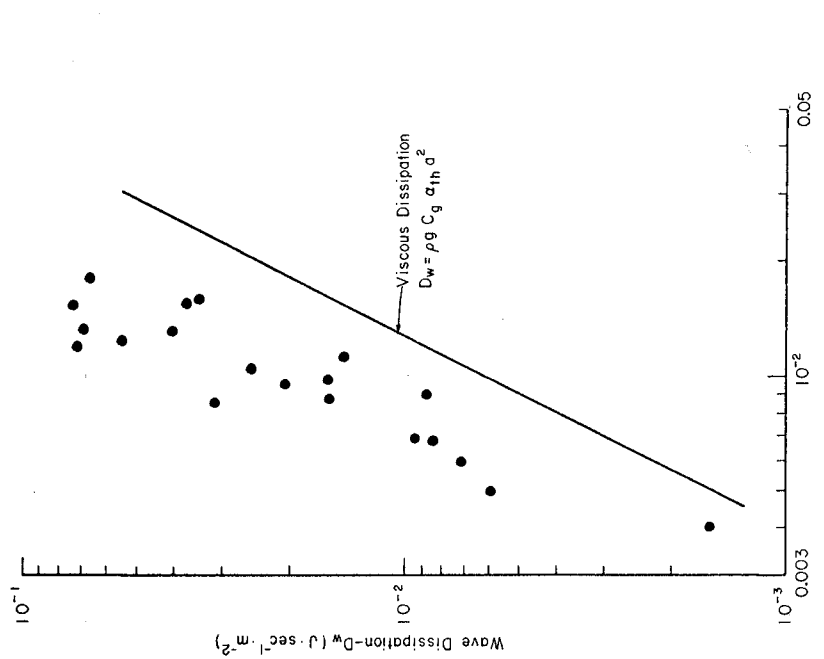

Figure 5. Still water wave dissipation

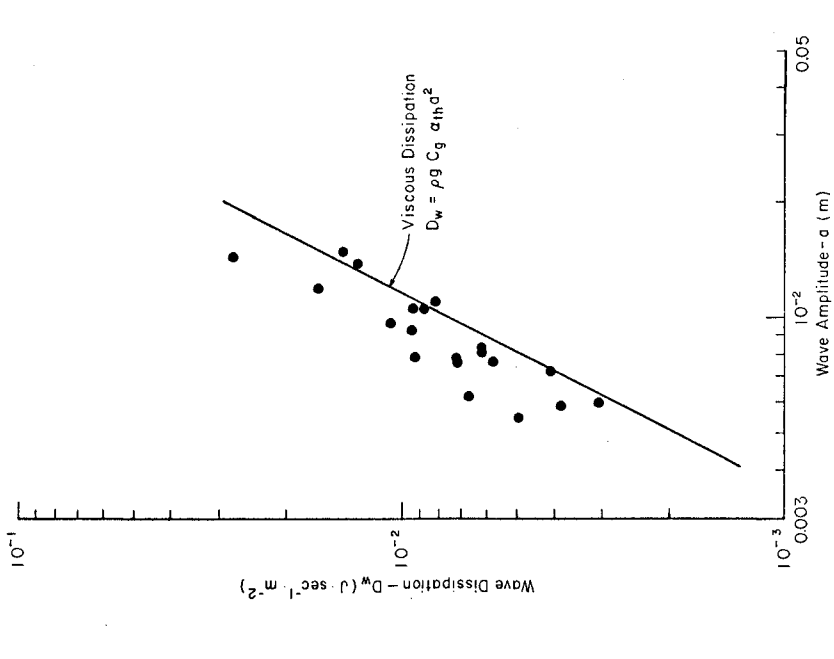

Figure 6. Wave dissipation on a turbulent flow.

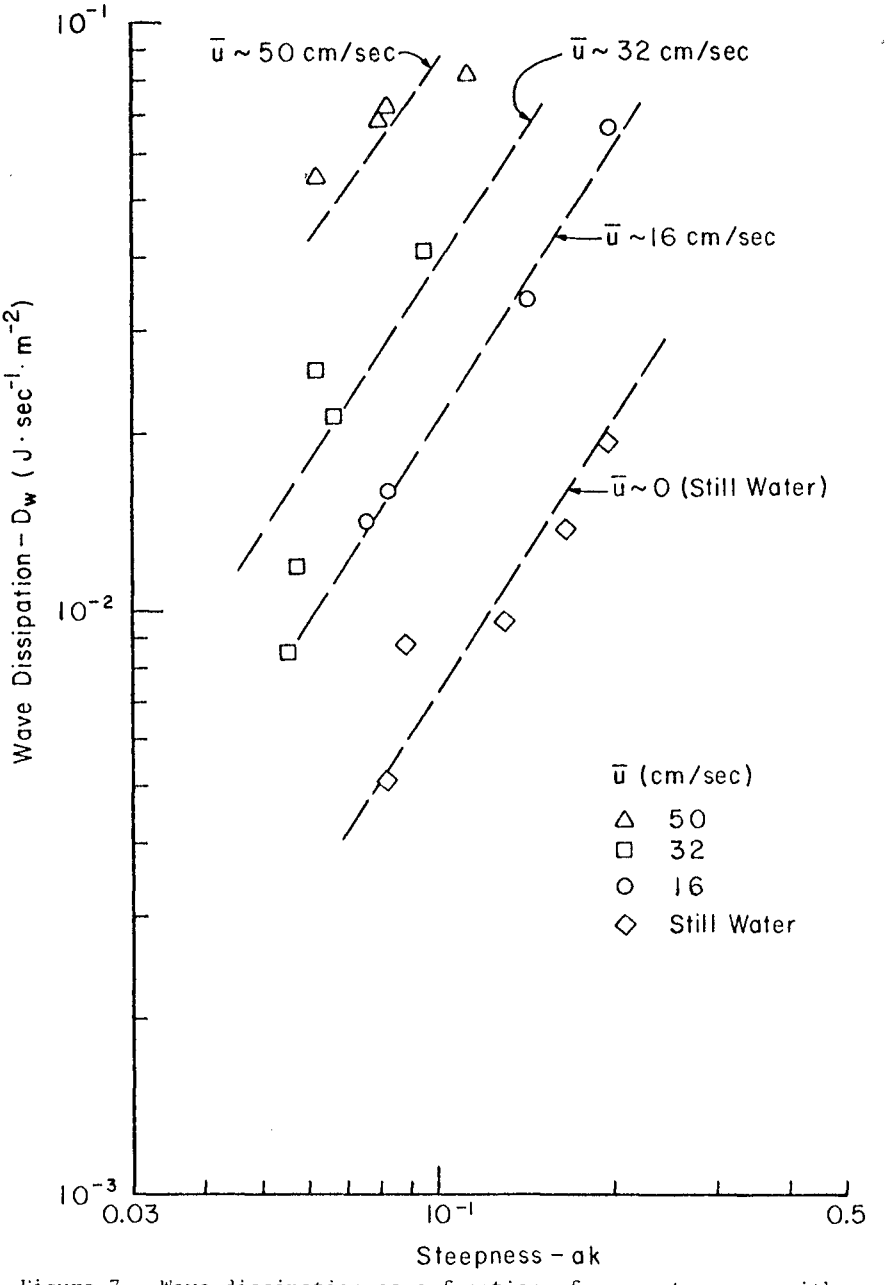

Figure 7. Wave dissipation as a function of wave steepness with constant flow velocity.

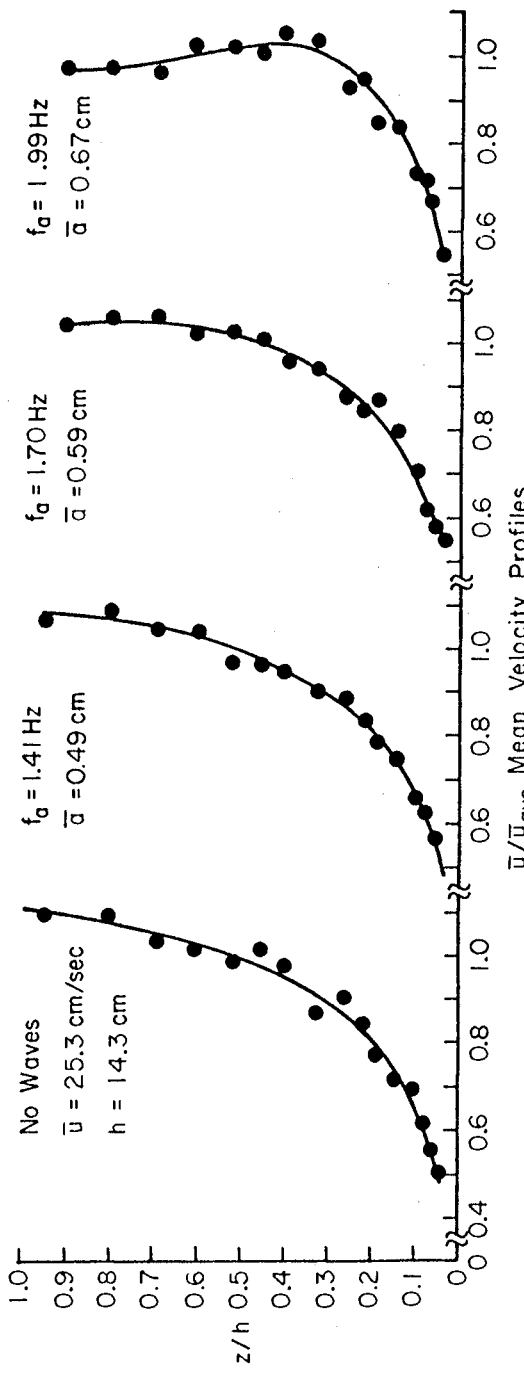

Figure 8. Mean velocity profiles with increasing wave frequency and amplitude.

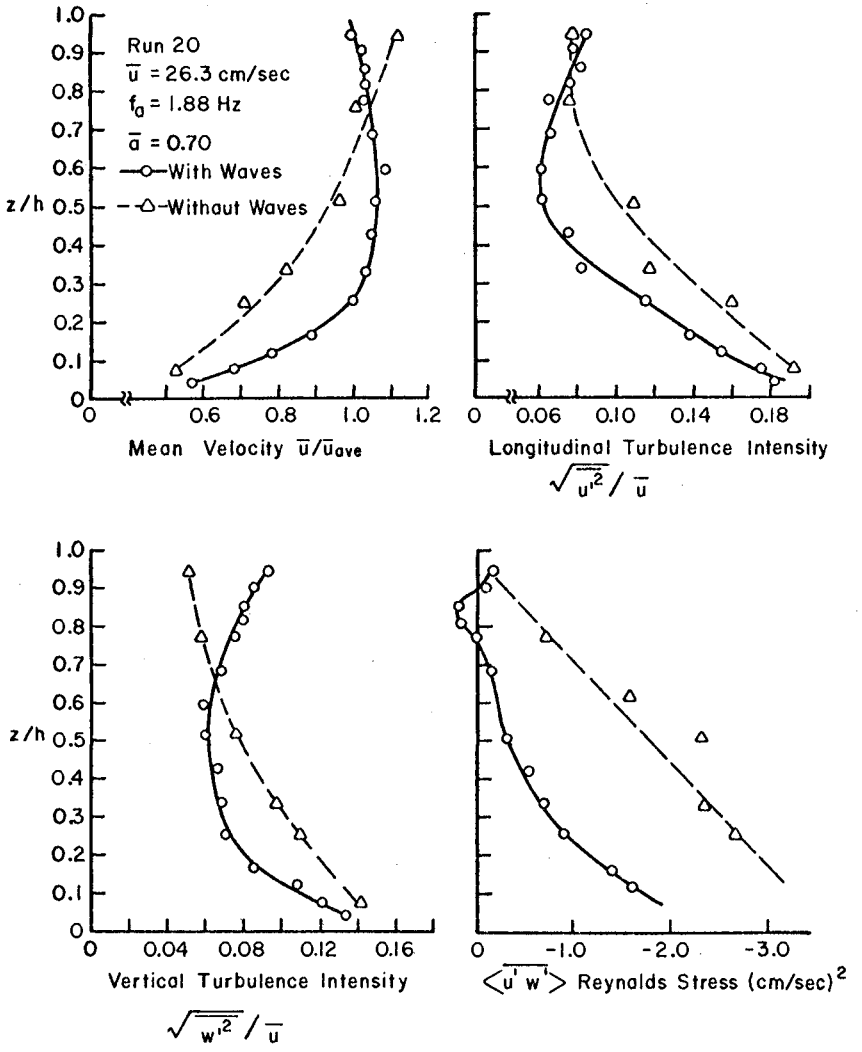

Figure 9. Mean velocity and turbulence profiles with and without waves.

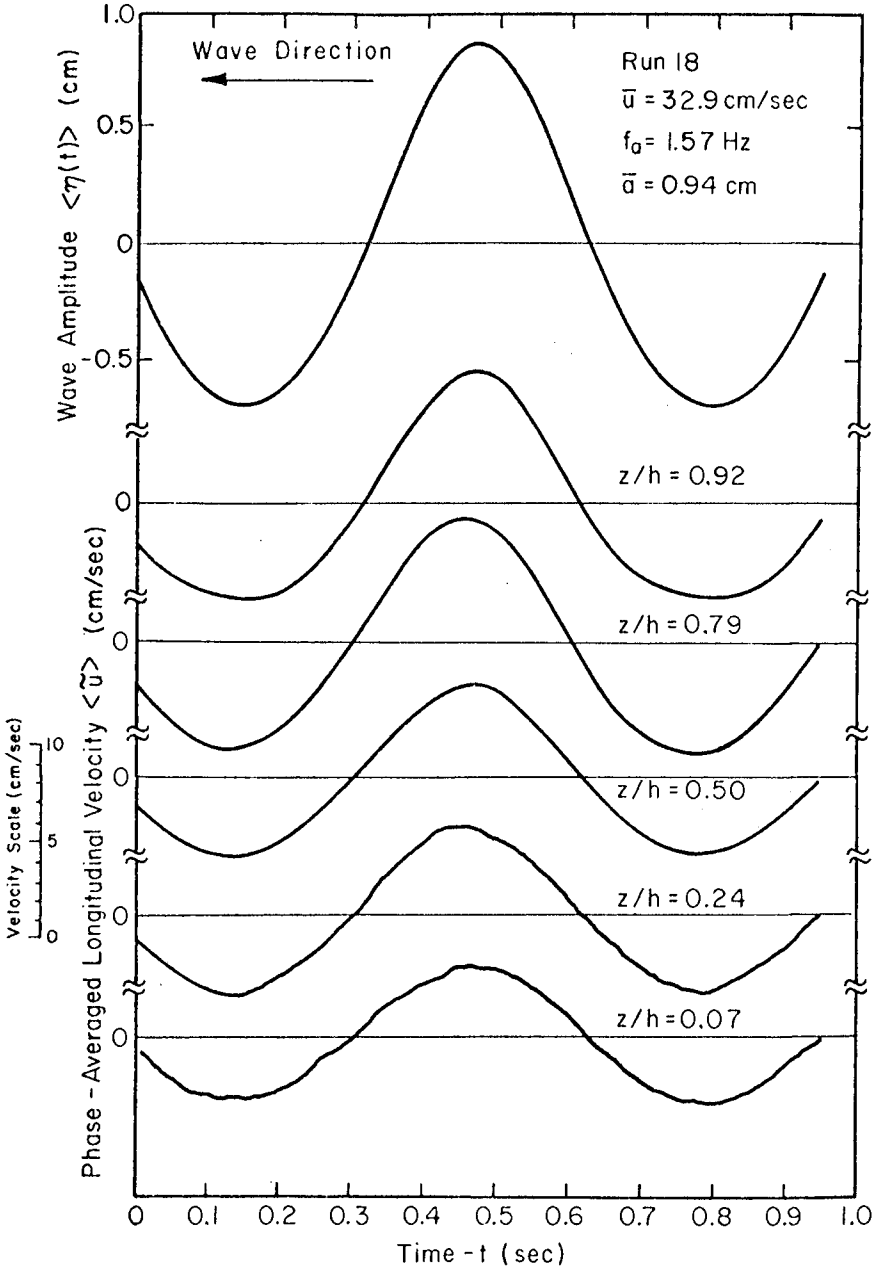

Figure 10. Phase averaged wave induced velocity $\langle\tilde{u}\rangle$.

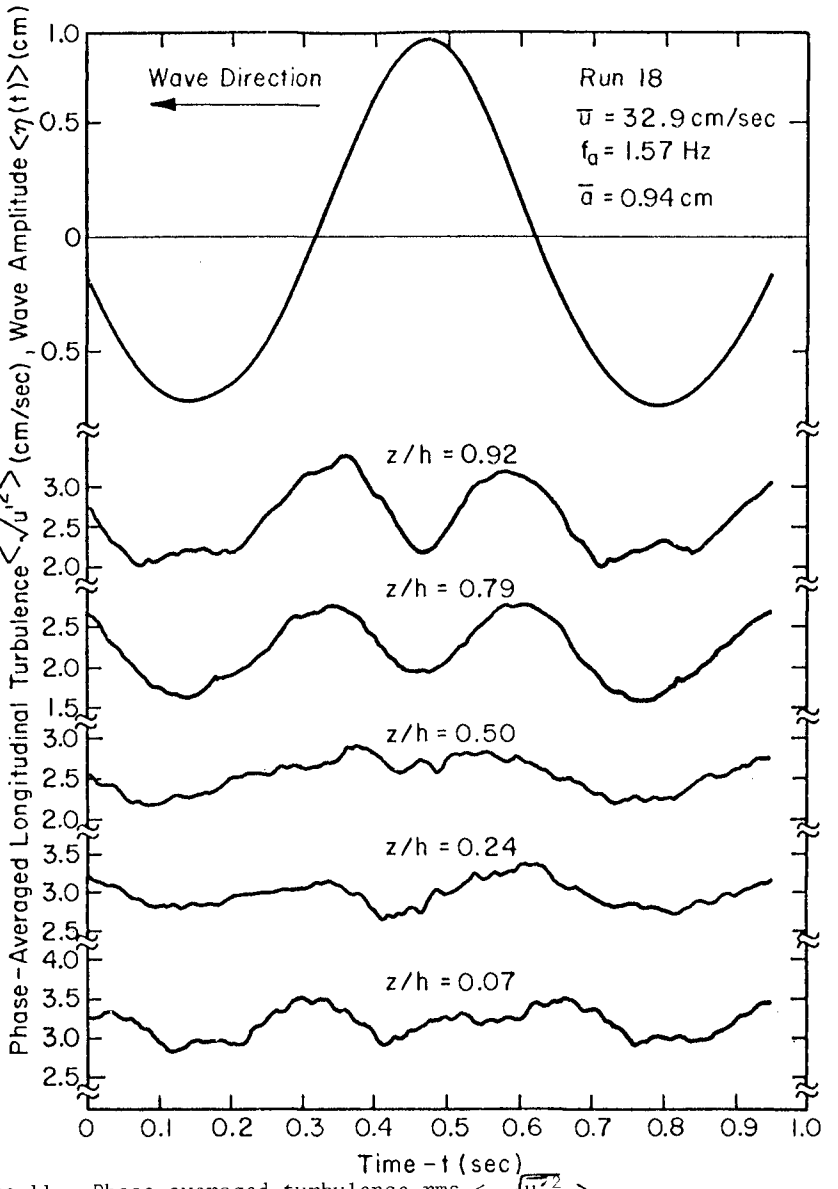

Figure 11. Phase averaged turbulence rms $\langle \sqrt{u'^2} \rangle$.

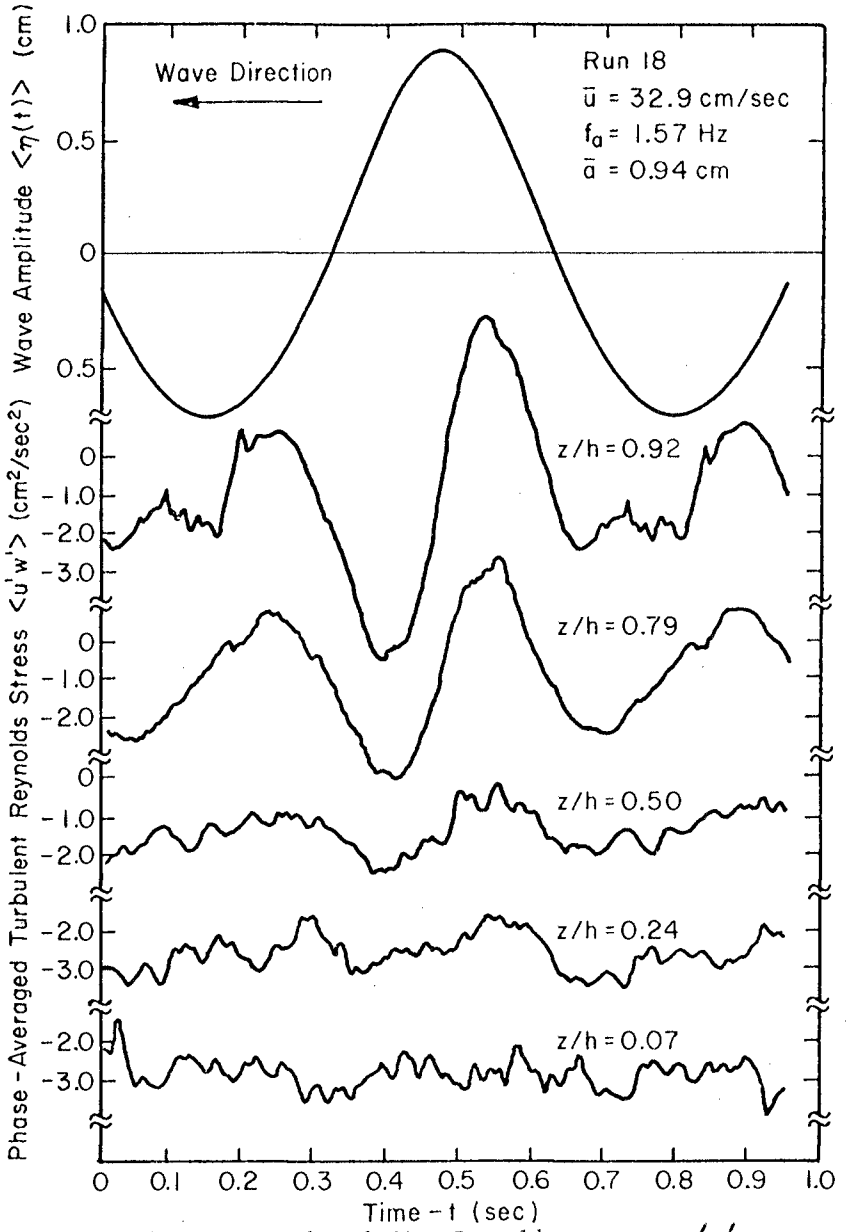

Figure 12. Phase averaged turbulent Reynolds stress $\langle u'w'\rangle$.

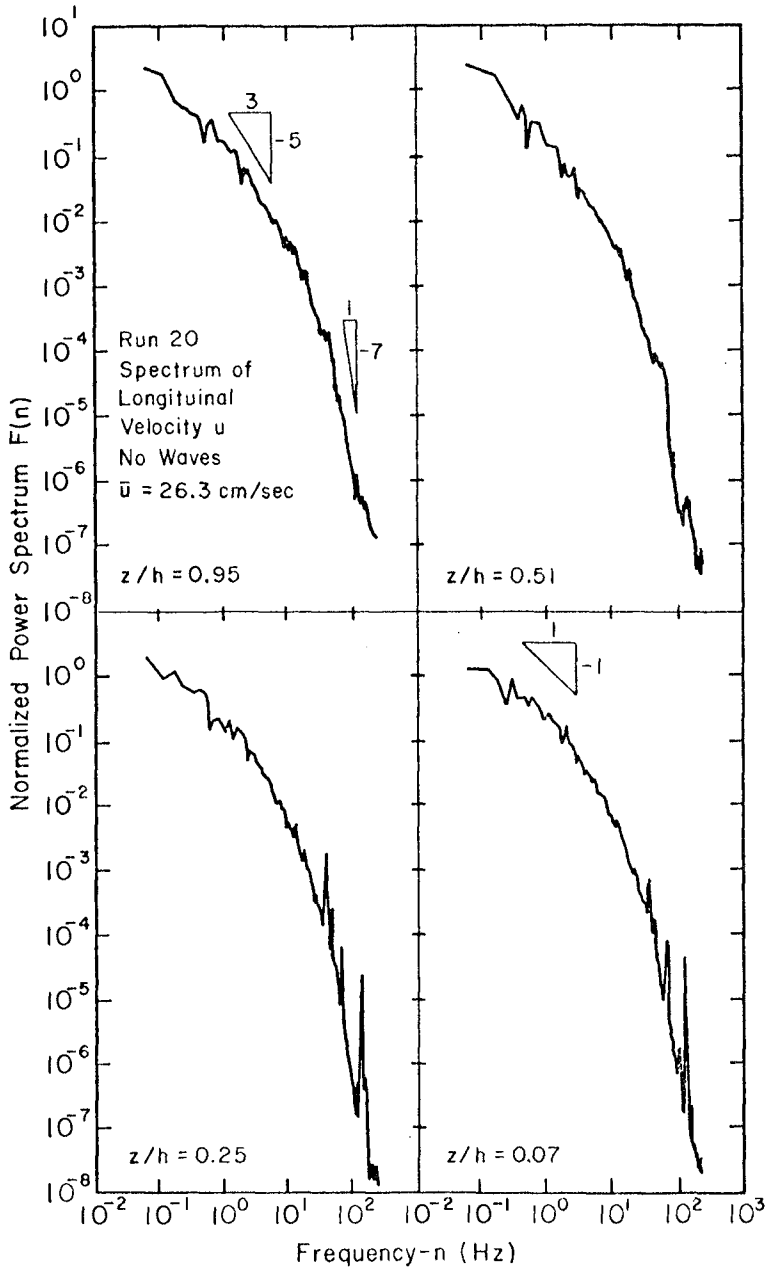

Figure 13. Spectra of longitudinal velocity, u, without waves.

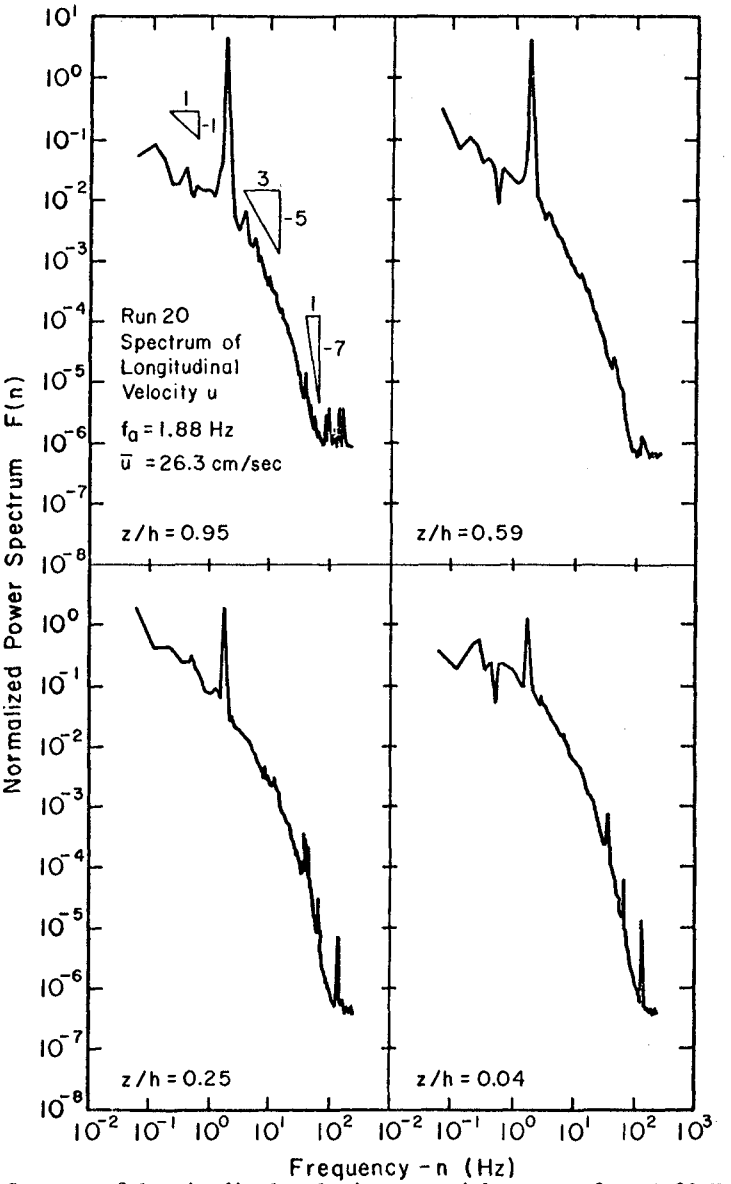

Figure 14. Spectra of longitudinal velocity, u, with waves, f_a = 1.88 Hz.